A Catalog of Regional Moment Tensors in Utah from 1998 to 2011

by Katherine M. Whidden and Kristine L. Pankow

Online Material: The electronic supplement includes details for all 48 moment tensor solutions in this study, including waveform fits and a table of event parameters.

INTRODUCTION

The University of Utah Seismograph Stations (UUSS) operates regional seismic networks in and around Utah and Yellowstone National Park and provides routine earthquake locations and earthquake catalogs for these two areas (Pechmann *et al.*, 2007). In this study, we expand the reporting to include moment tensors for seismic events occurring in the Utah region (Fig. 1). This region is a complex seismic environment with diverse source types: tectonic earthquakes, mining-induced seismicity (MIS) including mine collapses, and man-made sources such as explosions. Most tectonic earthquakes in the region occur within the Intermountain Seismic Belt (ISB; Smith and Arabasz, 1991). In northern Utah, the ISB roughly delineates the boundary between the Basin and Range and the Middle Rocky Mountains, whereas in central and southern Utah, the ISB separates the actively extending Basin and Range from the more stable Colorado Plateau. The MIS is mostly associated with long-wall coal mining in central Utah (Fig. 1; Arabasz *et al.*, 2007). The man-made blasts occur throughout the state and are related to both surface mining operations and military munitions detonations (Arrowsmith *et al.*, 2008).

Moment tensor inversion relies on broadband data and is usually possible for Utah seismic events of local magnitude (M_L) 3.5 and greater occurring after 1997. The first broadband instruments in the Utah region were installed in the mid-1990s, but this network was sparse. Prior to 1998, there were moment tensors for either large events, such as the 1992 M_w 5.5 St. George earthquake (Ritsema and Lay, 1995), or select events in northern Utah that were part of a 1994–1998 moment tensor catalog of the Pacific Northwest (Oregon State University).

Our aim is to develop a catalog of $M_L \geq 3.5$ regional moment tensors for the Utah region, allowing us to quantify and distinguish source types, gain a better understanding of the regional seismotectonics, improve upon current focal-depth information from network travel times, and enlarge the number of reliable estimates of moment magnitude (M_w) for use in seismic hazard analyses. In this paper, we (1) evaluate a suite of velocity models for suitability in the Utah regional moment tensor inversion; (2) calculate moment tensors for events in the Utah region with M_L 3.5 or greater from 1998 to mid-2011, extending to smaller events in a few select cases; and (3) evaluate all events for the presence of a significant isotropic component using a statistical F-test.

DATA PREPARATION AND METHODOLOGY

We implement the time-domain, full-waveform, least-squares moment tensor inversion of Minson and Dreger (2008), which is capable of calculating the full moment tensor, including double-couple, compensated linear vector dipole, and isotropic components. This method is well established and has been widely used in regional moment tensor studies worldwide, including South Africa (Brandt and Saunders, 2011), New Zealand (Ristau, 2008), Japan (Kubo *et al.*, 2002), and Brazil (Assumpção *et al.*, 2011). The full moment tensor capability of this method has been utilized to determine whether certain events have isotropic components, such as known and suspected nuclear explosions (Dreger and Woods, 2002; Ford *et al.*, 2009; Shin *et al.*, 2010), suspected mine-collapse events (Ford *et al.*, 2008), source processes of volcanic events (Dreger *et al.*, 2000; Templeton and Dreger, 2006; Cannata *et al.*, 2009), and glacial icequakes (Walter *et al.*, 2009, 2010). This ability to determine a volume-change component is especially important for the mining areas in Utah, where implosive events can occur (Fletcher and McGarr, 2005; Ford *et al.*, 2008).

Moment tensors for each event are determined by matching synthetic and data waveforms. Green's functions are calculated using frequency–wavenumber integration (Saikia, 1994) and then combined linearly into synthetics, in which the moment tensor elements determine the relative contribution of each fundamental Green's function to the final synthetic seismogram. Broadband three-component data from at least two stations are instrument corrected to displacement and downsampled to 1 sample/s, after which the horizontal components are rotated into radial and transverse directions. A band-pass filter of either 10–20 s (for $M_L < 4.5$) or 20–50 s (for $M_L \geq 4.5$) is then applied to both the data and the Green's functions; the long-period filter allows for a point-source assumption. Typically, a post-filter signal-to-noise ratio (SNR)

doi: 10.1785/0220120046

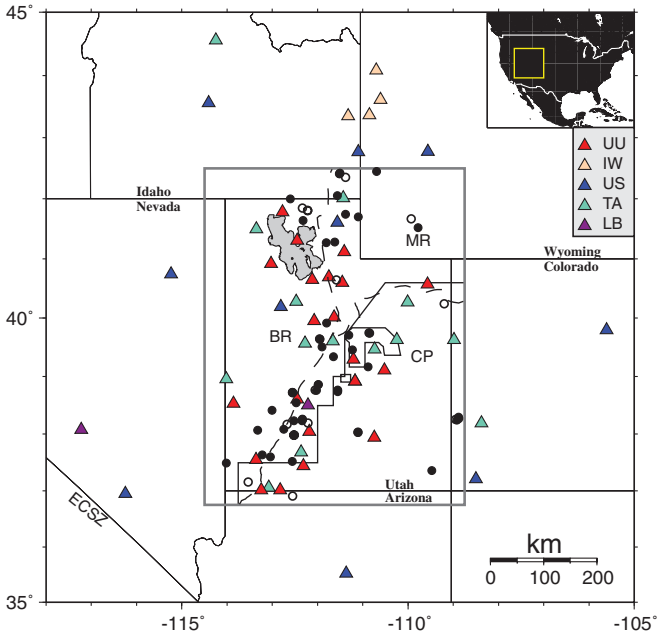

▲ **Figure 1.** UUSS Utah monitoring area (dark gray box) and the surrounding region. Solid black line separates the UUmod velocity model regions between Basin and Range to the northwest and Colorado Plateau to the southeast. Dashed line separates physiographic provinces: Basin and Range (BR), Colorado Plateau (CP), and Middle Rocky Mountains (MR). The transition zone is roughly the overlap between the physiographic and velocity model boundaries between the Basin and Range and Colorado Plateau in Central Utah. Crescent-shaped and rectangular polygons in central-eastern Utah are coal mining areas. ECSZ is the Eastern California Shear Zone. Triangles are broadband stations used in this study, colored by network as shown in legend at the top right: University of Utah Seismic Network (UU), Intermountain West Seismic Network (IW), U.S. National Seismic Network (US), EarthScope Transportable Array (TA), and Leo Brady Seismic Network (LB). Solid circles, epicentral locations for successful moment tensor; open circles, locations for moment tensors attempted but failed. This band of seismicity is the ISB in the Utah region.

of 3/1 is considered to eliminate noisy stations. Synthetic seismograms are shifted in time to best correlate with the data. These small time adjustments (dt) are necessary at each station to account for inaccuracies in the 1D velocity model. All three components at one station have the same dt value, and dt is limited to half of the shortest period in the filter or to 5 s.

To determine an optimum depth for each event, a suite of inversions at fixed depths is calculated, and the depth corresponding to the inversion with the highest variance reduction (VR), a measure of goodness of fit, is selected.

$$\mathrm{VR} = \left(1 - \sum_i \frac{\sqrt{(d_i - s_i)^2}}{\sqrt{d_i^2}}\right) * 100, \qquad (1)$$

in which d_i and s_i are the data and synthetic waveforms, respectively, at time i. A higher VR indicates a better fit of the synthetics to the data, with VR = 100% indicating a perfect fit. In this study, we require a minimum VR of 70% for a successful solution. Another measure of fit that can be used to constrain depth and is applicable when an isotropic component is not expected (an isotropic component can be ruled out by a statistical F-test, which will be discussed later) is the ratio of the residual to percent double couple (res/Pdc). Figure 2 illustrates the difference between VR and res/Pdc in an example from event number 43 (Ⓔ Table S1, available in the electronic supplement to this paper).

$$\frac{\mathrm{res}}{\mathrm{Pdc}} = \frac{\sum_i \sqrt{(d_i - s_i)^2}}{\mathrm{Pdc}}. \qquad (2)$$

Although VR may be flat over a range of depths, res/Pdc typically has a more distinct minimum. VR is used to determine the overall suitability of the solution, whereas res/Pdc is often used to determine depth. The maximum VR and minimum res/Pdc often coincide at the same or similar depth.

Before routine moment tensor processing began, we performed a quality assessment of the installed software and our processing methods. Using sample datasets and moment tensor solutions provided with the software, we ensured that we could match the example solutions.

VELOCITY MODEL TEST AND SELECTION

We examine preexisting velocity models and determine the best one for the regional moment tensor inversion in Utah.

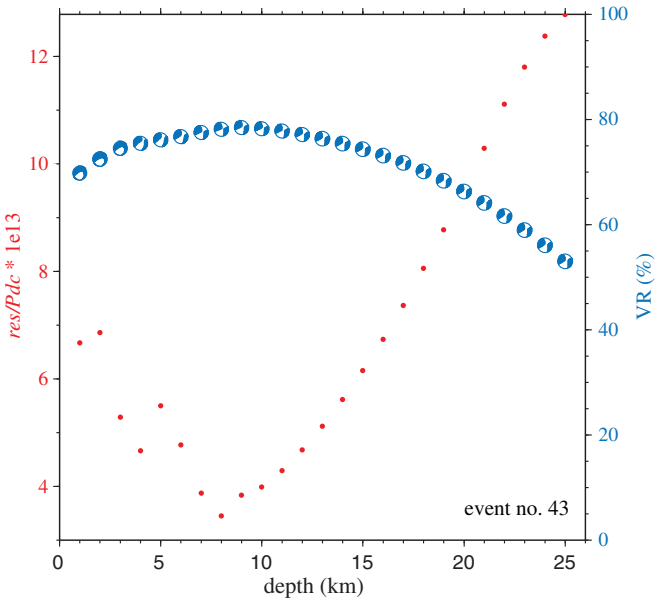

▲ **Figure 2.** Depth versus VR (focal mechanisms, right y axis, blue) and res/Pdc (circles, left y axis, red) for event number 43 (Ⓔ Table S1 in the supplement). VR has a broad high centered on 9-km depth, but res/Pdc shows a low at 8 km. In this case, we picked 8 km to be the best depth, preferring a higher percentage of double couple to absolute best fit.

Three velocity models are tested in this study, including one with two specified regions of applicability (Fig. 3). SONG (Song *et al.*, 1996) is a simple model consisting of two layers over a half-space and has been used successfully for moment tensors in Utah (Ford *et al.*, 2008) and Nevada (Dreger and Woods, 2002; Ford *et al.*, 2009). WUS is based on a velocity model used by the UUSS to locate earthquakes in the Yellowstone region, with adjustments to fit surface-wave dispersion curves, and has been used in the western United States, including Utah, for regional moment tensor inversion (Herrmann, Benz, and Ammon, 2011). UUmod is the velocity model used at UUSS for earthquake location (Roller, 1965; Keller *et al.*, 1975; Richins *et al.*, 1987). UUmod is based on *P*-wave refraction and consists of two 1D velocity models: (1) UUmod(BR) for events in the Basin and Range, transition zone to the Colorado Plateau, and Middle Rocky Mountain and (2) UUmod (CP) for events in the Colorado Plateau (Fig. 1). Attenuation (Q) for WUS can be found in the paper of Herrmann, Benz, and Ammon (2011), and Q-values for SONG are from Patton and Taylor (1984). UUmod Q-values are based on the WUS values.

We evaluate the three velocity models by calculating three full moment tensors for every event, one for each velocity model, using the same data for each of the three inversions, that is, same stations and same data window at each station. For each event, the VR resulting from inversions using the different velocity models is then evaluated as a ratio for the three model pairs: WUS/UUmod, SONG/UUmod, and WUS/SONG. The VR ratios for each model pair are ordered in decreasing value, assigned a sequential event number (from highest to lowest VR ratio; note that this event number does not match that in Ⓔ Table S1 in the supplement), and plotted as shown in Figure 4. Note that the resulting event numbers for each model pair differ, so events are not represented in the same order on the three ratio plots in Figure 4. If more events are above the equal ratio line ($y = 1$), then the numerator model has better VR results than those of the denominator model. Figure 4a and Figure 4b show that WUS and SONG produce better ressults than do the UUmod for a majority of events (75% and 66%, respectively). Furthermore, Figure 4c shows that WUS produces better results than does SONG for 68% of events. Because the assignment of a submodel (BR or CP) when using UUmod is based on epicentral location, the effect of regional sensitivity between these two submodels is also tested. In Figure 4a and Figure 4b, VR ratios using UUmod(BR) are plotted with black symbols and those using UUmod(CP), with gray. WUS produces better results than does UUmod(CP) in all cases, but SONG compared with UUmod(CP) yields better results for only about half of these events.

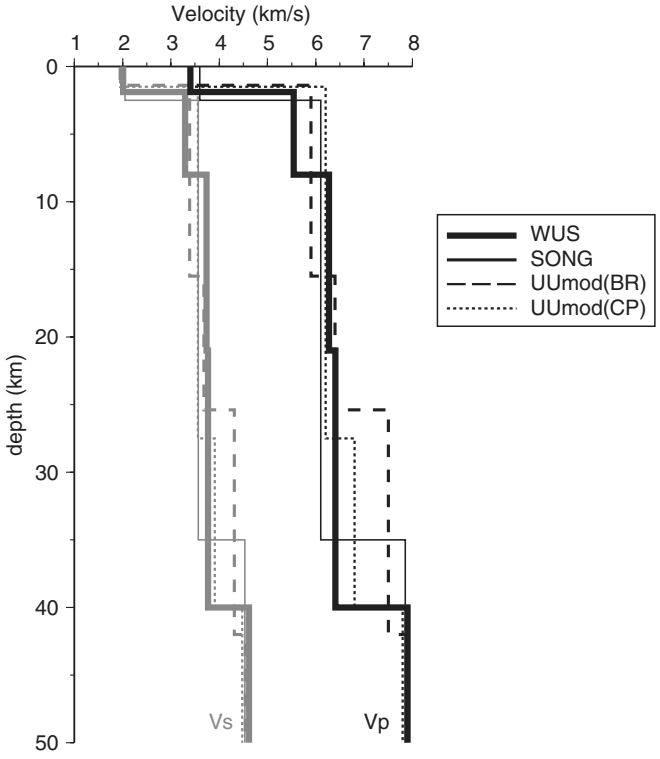

▲ **Figure 3.** Velocity models used in this study. For UUmod, different 1D models are shown: BR for the Basin and Range, transition zone region, and Middle Rocky Mountains and CP for the Colorado Plateau. Black line, V_P; gray line, V_S.

Events were also sorted north to south and east to west to look for geographic sensitivities, and it was found that SONG performs poorly in the eastern domain compared with the other two models, which could indicate that SONG is not appropriate for the Colorado Plateau. Because SONG was developed for the Basin and Range, its poor performance in a different geologic province is not unexpected. The north–south analysis revealed that UUmod performs best in the northern part of our study area. One possible explanation for the lower VR from UUmod compared with WUS and SONG is that the *P*-wave refraction analyses used to develop UUmod are less sensitive to the shallow, low-velocity layer that controls the Rayleigh waves, which dominate the moment tensor inversion at long periods (Song *et al.*, 1996). In summary, WUS results in the highest VR for most events, and for consistency, this model is used for the catalog presented here and will be used in future moment tensor inversions at UUSS.

STATISTICAL SIGNIFICANCE OF THE ISOTROPIC COMPONENT

We calculate full and deviatoric moment tensors for each event and then use a statistical F-test to determine whether each event has a significant isotropic component. The F-test compares the variance between a full and a deviatoric moment tensor weighted by the ratio of the degrees of freedom (DOF) in the inversion.

$$\mathrm{DOF} = \sum_{s} \left(\frac{pm}{f_c} \right) - u - 1, \tag{3}$$

in which p is the number of data points, s is the number of stations, m is the number of components, f_c is the filter corner frequency in seconds, and u is the number of unknowns in the

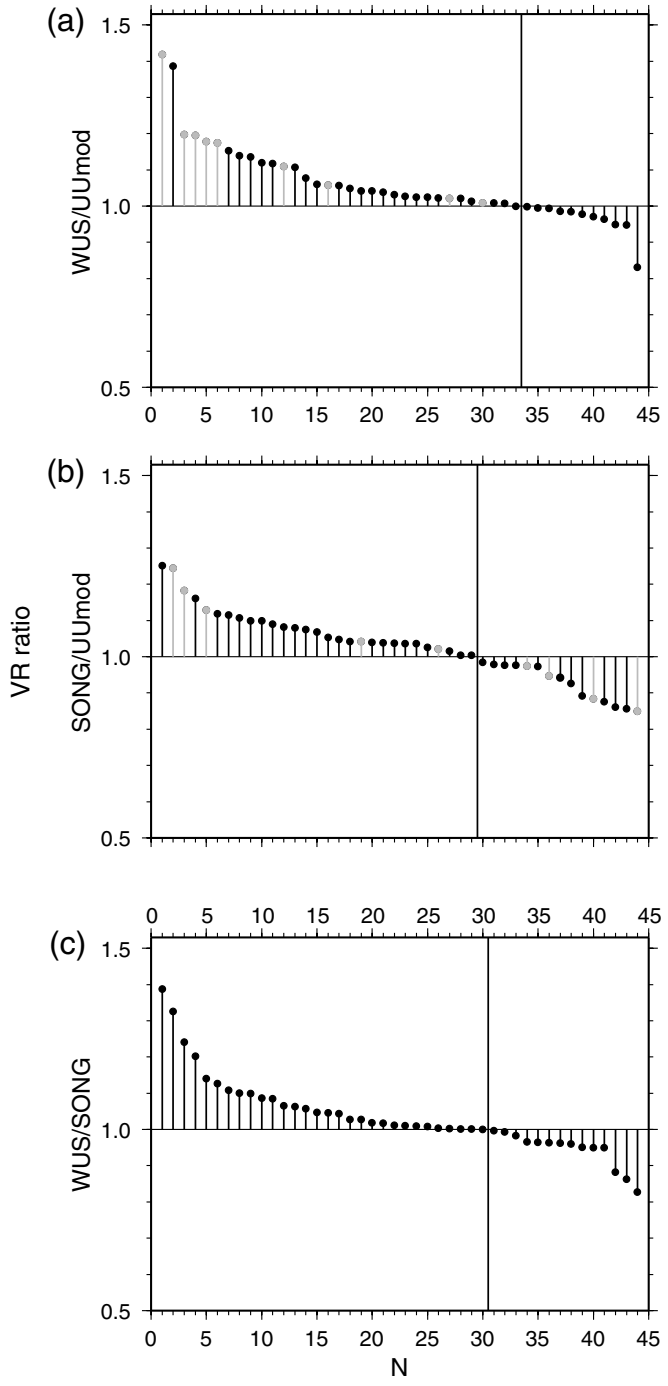

▲ **Figure 4.** Comparison of VR ratios versus event number for combinations of the three primary velocity models. For each model pair, the event number represents a sequential ordering of VR ratios from highest to lowest. VR > 1.0 indicates that the numerator model in the ratio produces better results; vertical lines demarcate the change from VR > 1 to VR < 1. In panels a and b, black lines denote UUmod(BR) and gray line denote UUmod(CP).

inversion (Dreger *et al.*, 2000; Panning *et al.*, 2001; Dreger and Woods, 2002; Templeton and Dreger, 2006). Because f_c is expressed in seconds rather than hertz, DOF decreases with a lower frequency filter. Using the ratio of variances (F-ratio; Menke, 1989) and degrees of freedom, a critical F-value is calculated. Because the number of points used at each station varies depending on data quality and event size, the degrees of freedom and therefore critical F-values vary with each event. From the critical F-value for each event, the statistical significance of the solution with greater VR but more DOF is calculated using routines in MATLAB (2009). F-test results are included with the event parameters (see Ⓔ Table S1 in the supplement). Panning *et al.* (2001) used synthetic data with known input sources to investigate the resolvability of isotropic moment tensor components and found that sources with no isotropic input have F-test results at the 75% confidence level or less, and sources with true isotropic input have F-test results at the 99% confidence level. Two events in our study (numbers 10 and 32, both F-tests 100%, Ⓔ Table S1 in the supplement) meet the criteria for isotropic component significance and will be discussed in detail in the next section.

RESULTS

Using the WUS velocity model, moment tensor inversions for all events in the UUSS catalog for the Utah region from 1998 to mid-2011 reported with $M_L \geq 3.5$ are attempted, and successful solutions for 44 of 63 events are obtained (70%). The resulting source parameters for these 44 successful events and 4 additional events with $M_L < 3.5$ are presented in Ⓔ Table S1 (see supplement). Waveform fits for each event are available as an Ⓔ electronic supplement to this paper. The moment tensor results show focal mechanisms ranging from normal to strike slip (Ⓔ Fig. 5, as well as the 48 waveform fit figures in the electronic supplement). Figure 6 is a histogram of counts of attempted and successful events by event magnitude. Unsuccessful attempts are due to poor station coverage, large event-to-station distances (primarily before broadband-station coverage increased in the area), strong microseism noise, or teleseism interference. For example, a M_L 4.0 earthquake in 2009 was contaminated with low-frequency energy from a M_w 5.6 earthquake in Mexico. More often, poor SNR at the frequencies used for moment tensor inversion is the cause of failed attempts for smaller events.

We are able to obtain moment tensors for four events with $M_L < 3.5$. In these cases, there are two or more stations within 85 km of the epicenter, and fortuitously, the microseism amplitudes are relatively low. The $M_L < 3.5$ events are attempted as special cases rather than as part of the routine moment tensor processing, so we do not include them in our completeness statistics and they are not represented in Figure 6. The special cases include two small events in regions of known MIS and two events that generated significant public interest. Focal mechanisms for these smaller events are shown in blue in Figure 5.

DISCUSSION

We use T-axes from moment tensors in this study to examine stress orientations in the Utah region and compare our results with those of other studies. T-axes for the focal mechanisms

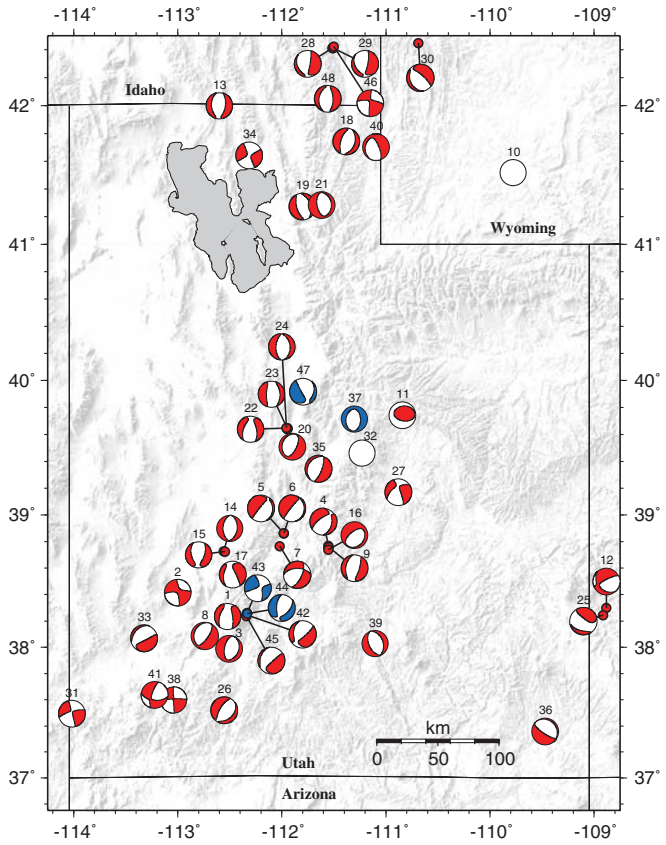

▲ **Figure 5.** Utah moment tensors calculated in this study. Red, events with M_L ≥3.5; blue, M_L <3.5. Numbers above focal mechanisms correspond to ID, Ⓔ Table S1 (see supplement).

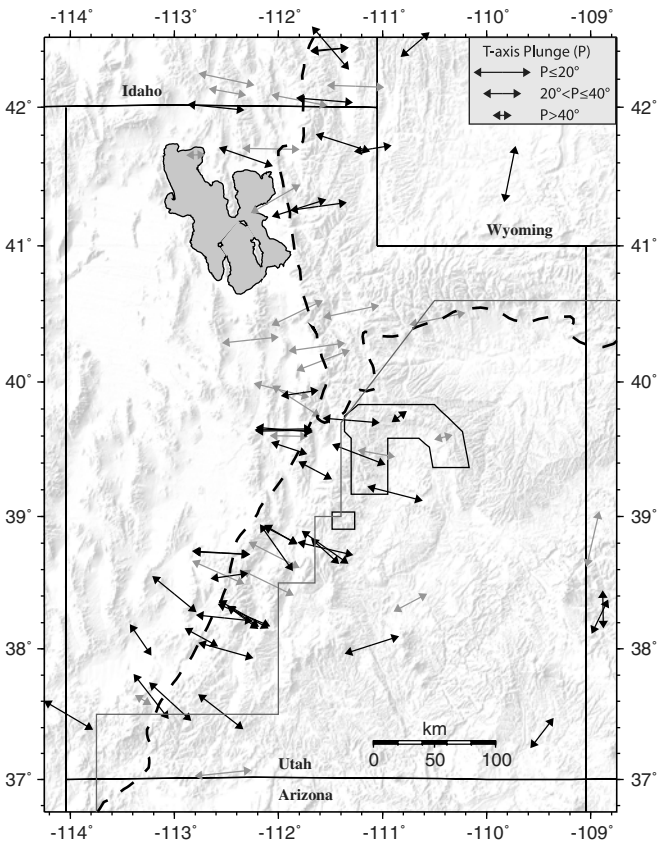

▲ **Figure 7.** *T*-axes derived from moment tensors in this study (black) and quality A, B, and C data from the World Stress Map Project (gray; Heidbach *et al.*, 2008). Arrows are scaled by axis plunge (see legend, top right). Physiographic and velocity model boundaries and mining area polygons are the same as those in Figure 1.

shown in Figure 5 are plotted as black arrows in Figure 7 and reveal a difference in stress orientation between the Basin and Range (western and central Utah) and the Colorado Plateau (eastern Utah and western Colorado). Gray arrows in Figure 7 are *T*-axes from the World Stress Map Project (e.g., Heidbach *et al.*, 2009 and references therein), a compilation of many studies that, in the data represented here, includes stress orientations from single earthquake focal mechanisms, geologic fault-slip data, and borehole breakouts. The *T*-axes from our study are consistent with the World Stress Map compilation data.

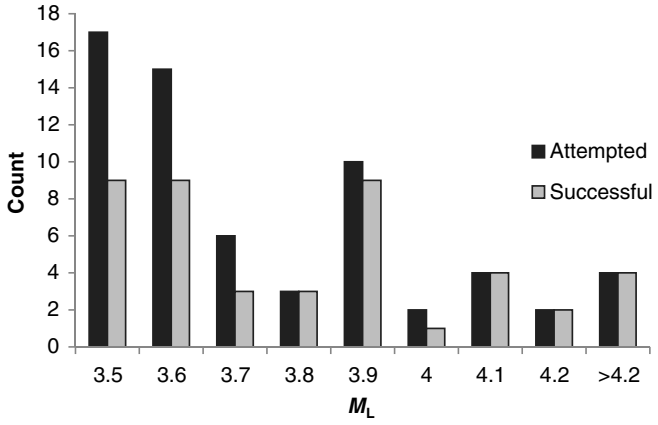

▲ **Figure 6.** Successful and failed moment tensor solutions. Moment tensors are attempted for all 63 events reported with M_L ≥3.5 in the study region from 1998 to mid-2011.

Along the ISB, *T*-axes indicate roughly east–west extension in northern and central Utah, with a rotation to northwest–southeast extension, perpendicular to the Basin and Range–Colorado Plateau boundary in southwestern Utah. The rotation in *T*-axes in southwestern Utah corresponds with an increase in strike-slip and oblique mechanisms (Fig. 5). Arabasz *et al.* (2007) noted that heterogeneous focal mechanisms in the Basin and Range–Colorado Plateau transition in south-central Utah are suggestive of a transitional stress regime between normal and strike-slip faulting, in which the vertical and horizontal maximum compressive stresses are similar in magnitude and the orientation of maximum compressive stress may interchange from event to event. The change in stress orientation in southwestern Utah has also been noted by Pankow *et al.* (2009), who suggested that the rotation of *T*-axes is the result of partitioning of extension across preexisting transform structures (e.g., Duebendorfer and Black, 1992; Rowley *et al.*, 1997).

Kreemer *et al.* (2010) proposed that these transform structures and associated seismicity provide evidence for a kinematic connection in southern Nevada between the ISB and the Eastern California shear zone.

We briefly compare our results with two other moment tensor catalogs with which we have solutions in common: (1) a double-couple moment tensor study of North America by Herrmann, Benz, and Ammon (2011; 27 common events) and (2) a mid-1990s moment tensor study of the Pacific Northwest (Oregon State University; three common events). We focus the comparison on the Herrmann, Benz, and Ammon (2011) study because of the larger number of common events and because the North American study is more recent and ongoing. We find two (numbers 10 and 32, Ⓔ Table S1 in the supplement) of the 27 events in common with Herrmann, Benz, and Ammon (2011) to have significant isotropic components and therefore leave them out of the comparison. Of the remaining 25 solutions, 13 (52%) have T-axes within 10° of each other, 20 (80%) within 20°, and five with dissimilar T-axes (> 20° difference). Of the five solutions with dissimilar T-axes, two (numbers 1 and 13, Ⓔ Table S1 in the supplement) appear to be due to a significant difference in best-depth selection; for the other three (numbers 11, 22, and 27, Ⓔ Table S1 in the supplement), the solutions are comparable, but there are significant rotations in the dips of the nodal planes. Figure 8 shows the close agreement in M_w between this study and Herrmann, Benz, and Ammon (2011). All three events in common with the Pacific Northwest study have T-axes within 20% of each other.

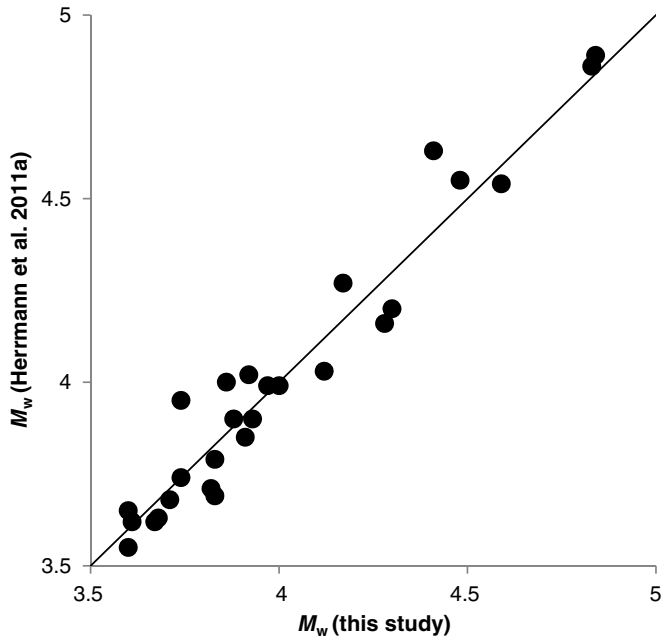

▲ **Figure 8.** Comparison of M_w for the 25 events in common between this study and Herrmann, Benz, and Ammon (2011). The solid line represents M_w (this study) = M_w (Herrmann, Benz, and Ammon, 2011).

One event (number 12) in our study is a velocity model special case. The event occurred in western Colorado on the far eastern edge of the UUSS monitoring region in 2000, before the regional broadband network was very extensive. Only two available stations recorded adequate data, although the event is fairly large at M_L 4.3. One station is to the east in central Colorado and the other to the west in central Utah. Usually, one velocity model is suitable for all stations in the moment tensor inversion, but for this event, data at the Colorado station are much better fit by UUmod(CP) and at the Utah station, by WUS (Fig. 9). By using Green's functions from the better-fitting model at each station, a successful moment tensor is obtained. Despite our preference to use a single velocity model for simplicity in routine processing, this event demonstrates the utility of using multiple velocity models when necessary.

We compare M_w from this study with M_L from the UUSS catalog (Fig. 10). Moment magnitudes in this study, computed using the standard Hanks and Kanamori (1979) relation, range from 3.2 to 4.6. The plot of M_w versus M_L shows little systematic bias, and the standard deviation from a line of $x = y$ is 0.2. Pechmann *et al.* (2007) similarly compared M_w calculated as part of multiple studies using multiple techniques with M_L from the UUSS catalog. They found systematic differences between the UUSS network M_L and the aggregate compilation of M_w but acknowledge that the differences could

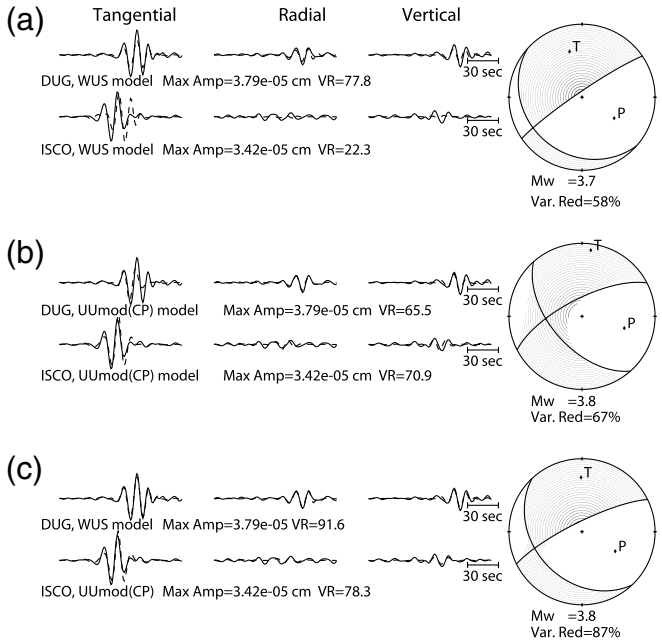

▲ **Figure 9.** Comparison of results using different velocity models for different stations, as indicated, to calculate moment tensors for event number 12, for which suitable data are available from only two stations: DUG and ISCO. Solid waveforms, data; dashed waveforms, synthetics. The resulting mechanisms, M_w, and VR are shown for the three cases. (a) Both stations modeled using WUS, similar to the other events in the study. (b) UUmod(CP) is used for both stations. (c) WUS model for station DUG and UUmod(CP) for station ISCO.

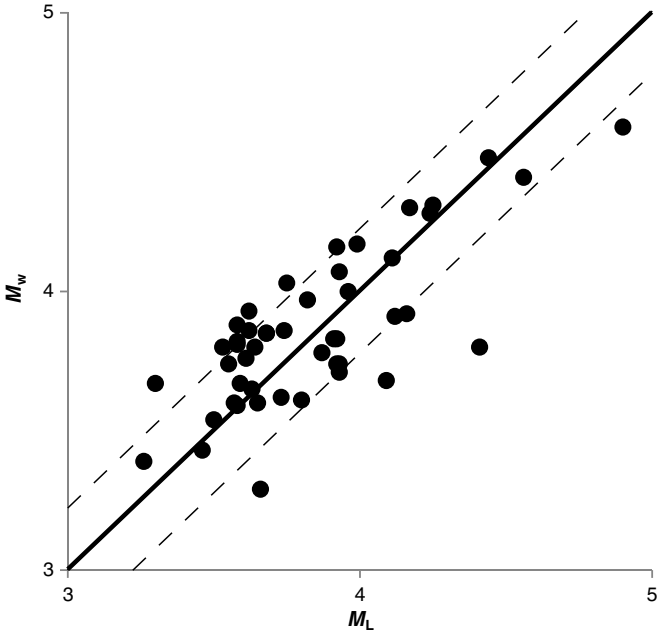

▲ **Figure 10.** M_w determined in this study versus M_L determined by UUSS. Solid line, $M_w = M_L$; dashed line, standard deviation of the data from the solid line (±0.2).

be due to the multiple methods and velocity models used to calculate the M_w values. Hanks and Boore (1984) found that the $M_w - M_L$ relation is nonlinear, whereas several other studies have found good correlation between M_w and M_L (Thio and Kanamori, 1995; Uhrhammer *et al.*, 1996; Zhu and Helmberger, 1996; Herrmann, Malagnini, Munafò, 2011). We will investigate the relationship between M_w and M_L in the Utah region more thoroughly in future work.

In our dataset, we identify two events with significant isotropic components; both are associated with failures in underground mines. One solution is for an event in southwestern Wyoming on 30 January 2000 (number 10, Ⓔ Table S1 in the supplement, M_w 4.3, *F*-test 100%), which is associated with a roof fall (collapse) involving three room and pillar sections in an underground trona mine (McCarter, 2001). The other solution (number 32, Ⓔ Table S1 in the supplement, M_w 4.2, *F*-test 100%) is for the well-documented August 2007 Crandall Canyon coal-mine collapse (see Pechmann *et al.*, 2008). Our solution for the Crandall Canyon event is similar to that of Ford *et al.* (2008). Before completing the *F*-test, we suspected that a third event (number 11, Ⓔ Table S1 in the supplement) might also have a significant isotropic component because it occurred within the Willow Creek coal mine, closely in time with seven reported roof falls (Ellenberger *et al.*, 2001; McCarter, 2001). This is one of the largest seismic events associated with underground coal mining in Utah (see Pechmann *et al.*, 2008). The full moment tensor solution has a relatively large isotropic component of 21% (not shown in Ⓔ Table S1 in the supplement as the deviatoric solution is the only one reported). However, the *F*-test result of 57% indicates that the full moment tensor solution is not significantly better than the deviatoric, so we cannot confirm that this event has a significant volume change. However, we also cannot rule out that the event has a real isotropic component that is very small compared with the deviatoric portion of the moment tensor. This latter alternative is consistent with the interpretation of a shear-slip event in the roof of the mine that triggered roof falls in the mine workings (Arabasz and Pechmann, 2001; Ellenberger *et al.*, 2001). Inversions of synthetic data similar to those by Panning *et al.* (2001) may be useful in developing thresholds for the *F*-test and in better understanding a potentially complicated source event such as this one. Without such testing, we are unable to distinguish an event with a small isotropic and large double-couple source from a purely deviatoric source.

CONCLUSIONS

We have developed a catalog of moment tensors for events in the UUSS Utah seismic monitoring region from 1998 to mid-2011. The moment tensor catalog contains 70% of the events reported with $M_L \geq 3.5$ in the UUSS earthquake catalog. Moment tensor calculation for events as small as M_w 3.2 (M_L 2.9) is possible with short event-to-station distances and favorable microseism conditions. We will explore the possibility of routinely analyzing events with $M_L < 3.5$ in future work. The WUS velocity model (Herrmann, Benz, and Ammon, 2011) results in the best moment tensor variance reduction for events in the Utah region and will be used in ongoing moment tensor analyses, although we have shown that in special circumstances it may be advantageous to use multiple velocity models.

Twenty-five moment tensors calculated in this study are generally similar to solutions for the same events determined by Herrmann, Benz, and Ammon (2011). Focal mechanisms for the moment tensors developed in this study are consistent with the results of previous studies on the regional tectonics and stress orientation (e.g., Zoback and Zoback, 1989; Arabasz *et al.*, 2007; Heidbach *et al.*, 2009; Pankow *et al.*, 2009; Kreemer *et al.*, 2010). Two events in our catalog have moment tensors with significant isotropic components as determined by the *F*-test and are associated with known mine collapses. The interpretation of an isotropic component in the moment tensor of a third noteworthy mining-related event is less conclusive. The full moment tensor analysis is essential for any region with diverse seismic sources such as Utah, particularly if MIS is routinely monitored.

ACKNOWLEDGMENTS

We thank Douglas Dreger and Taka'aki Taira for the moment tensor inversion code and associated programs, for their support in setting up the codes at University of Utah Seismograph Stations, and for the sample datasets, which allowed us to conduct a thorough quality assessment. We thank Walter Arabasz, Keith Koper, and an anonymous reviewer for constructive

reviews that improved the manuscript. We were partially supported by the State of Utah under a line-item appropriation to the University of Utah Seismograph Stations and by the United States Geological Survey (USGS), Department of the Interior, under USGS Award Number G10AC00085.

REFERENCES

Arabasz, W. J., R. Burlacu, and K. L. Pankow (2007). An overview of historical and contemporary seismicity in central Utah, *Utah Geol. Surv. Publ.* **36,** 237–253.

Arabasz, W. J., and J. C. Pechmann (2001). Seismic characterization for coal-mining seismicity in Utah for CTBT monitoring, Technical Report UCRL-CR-143772, Lawrence Livermore National Laboratory, Livermore, California, LLNL Research Agreement No. B344836, 102 pp., accessible at http://quake.utah.edu/Reports/llnl2001/ (last accessed July 2012).

Arrowsmith, S. J., R. Whitaker, S. R. Taylor, R. Burlacu, B. Stump, M. Hedlin, G. Randall, C. Hayward, and D. ReVelle (2008). Regional monitoring of infrasound events using multiple arrays: Application to Utah and Washington State, *Geophys. J. Int.* **175,** 291–300.

Assumpção, M., J. C. Dourado, L. C. Ribotta, W. U. Mohriak, F. L. Dias, and J. R. Barbosa (2011). The São Vicente earthquake of 2008 April and seismicity in the continental shelf off SE Brazil: Further evidence for flexural stresses, *Geophys. J. Int.* **187,** 1076–1088.

Brandt, M. B. C., and I. Saunders (2011). New regional moment tensors in South Africa, *Seismol. Res. Lett.* **82,** 69–80.

Cannata, A., M. Hellweg, G. Di Grazia, S. Ford, S. Alparone, S. Gresta, P. Montalto, and D. Patanè (2009). Long period and very long period events at Mt. Etna volcano: Characteristics, variability and causality, and implications for their sources, *J. Volcanol. Geoth. Res.* **187,** 227–249.

Dreger, D. S., H. Tkalčić, and M. Johnston (2000). Dilational processes accompanying earthquakes in the Long Valley Caldera, *Science* **288,** 122–125.

Dreger, D., and B. Woods (2002). Regional distance seismic moment tensors of nuclear explosions, *Tectonophysics* **356,** 139–156.

Duebendorfer, E. M., and R. A. Black (1992). Kinematic role of transverse structures in continental extension—An example from the Las Vegas shear zone, Nevada, *Geology* **20,** 1107–1110.

Ellenberger, J. L., K. A. Heasley, P. L. Swanson, and J. Mercier (2001). Three dimensional microseismic monitoring of a Utah longwall, in *Rock Mechanics in the National Interest*, D. Elsworth, J. P. Tinucci, and K. A. Heasley (Editors), A.A. Balkema, Rotterdam, The Netherlands, 1321–1326.

Fletcher, J. B., and A. McGarr (2005). Moment tensor inversion of ground motion from mining-induced earthquakes, Trail Mountain, Utah, *Bull. Seismol. Soc. Am.* **95,** 48–57.

Ford, S. R., D. S. Dreger, and W. R. Walter (2008). Source characterization of the 6 August 2007 Crandall Canyon Mine seismic event in central Utah, *Seismol. Res. Lett.* **79,** 637–644.

Ford, S. R., D. S. Dreger, and W. R. Walter (2009). Identifying isotropic events using a regional moment tensor inversion, *J. Geophys. Res.* **114,** no. B01306, 12 pp. doi: 10.1029/2008JB005743.

Hanks, T. C., and D. M. Boore (1984). Moment–Magnitude relations in theory and practice, *J. Geophys. Res.* **89,** 6229–6235.

Hanks, T. C., and H. Kanamori (1979). A moment magnitude scale, *J. Geophys. Res.* **84,** 2348–2350.

Heidbach, O., M. Tingay, A. Barth, J. Reinecker, D. Kurfeß, and B. Müller (2008). The World Stress Map database release 2008, doi: 10.1594/GFZ.WSM.Rel2008, stress data available at www.world-stress-map.org (last accessed July 2012).

Herrmann, R. B., H. Benz, and C. J. Ammon (2011). Monitoring the earthquake source process in North America, *Bull. Seismol. Soc. Am.* **101,** 2609–2625.

Herrmann, R. B., L. Malagnini, and I. Munafò (2011). Regional moment tensors of the 2009 L'Aquila earthquake sequence, *Bull. Seismol. Soc. Am.* **101,** 975–993.

Keller, G. R., R. B. Smith, and L. R. Braile (1975). Crustal structure along the Great Basin Colorado Plateau transition from seismic refraction studies, *J. Geophys. Res.* **80,** 1093–1098.

Kreemer, C., G. Blewitt, and W. Hammond (2010). Evidence for an active shear zone in southern Nevada linking the Wasatch fault to the Eastern California shear zone, *Geology* **38,** 475–478.

Kubo, A., E. Fukuyama, H. Kawai, and K. Nonomura (2002). NIED seismic moment tensor catalogue for regional earthquakes around Japan: Quality test and application, *Tectonophysics* **356,** 23–48.

MATLAB 7.8 (2009). The MathWorks Inc., Natick, Massachusetts.

McCarter, M. K. (2001). Documentation of ground truth for significant seismic events related to underground mining in Utah and Wyoming, in *Seismic Characterization of Coal-Mining Seismicity in Utah for CTBT Monitoring*, W. J. Arabasz and J. C. Pechmann (Editors), Technical Report UCRL-CR-143772, Lawrence Livermore National Laboratory, Livermore, California, accessible at http://quake.utah.edu/Reports/llnl2001/.

Menke, W. (1989). *Geophysical Data Analysis: Discrete Inverse Theory*, Academic Press, San Diego, California, 96–99.

Minson, S. E., and D. S. Dreger (2008). Stable inversions for complete moment tensors, *Geophys. J. Int.* **74,** 585–592.

Oregon State University, Moment–Tensor Catalogue, http://quakes.oce.orst.edu/moment-tensor/ (last accessed April 2012).

Pankow, K. L., W. J. Arabasz, and R. Burlacu (2009). Seismicity and seismotectonic issues of Western Utah, *Utah Geol. Surv. Publ.* **38,** 15.

Panning, M., D. Dreger, and H. Tkalčić (2001). Near-source velocity structure and isotropic moment tensors: A case study of the Long Valley Caldera, *Geophys. Res. Lett.* **28,** 1815–1818.

Patton, H. J., and S. R. Taylor (1984). Q structure of the basin and range from surface waves, *Geophys. Res. Lett.* **89,** 6929–6940.

Pechmann, J. C., W. J. Arabasz, K. L. Pankow, R. Burlacu, and M. K. McCarter (2008). Seismological report on the 6 August 2007 Crandall Canyon mine collapse in Utah, *Seismol. Res. Lett.* **79,** 620–636.

Pechmann, J. C., S. J. Nava, F. M. Terra, and J. C. Bernier (2007). Local magnitude determinations for intermountain seismic belt earthquakes from broadband digital data, *Bull. Seismol. Soc. Am.* **97,** 557–574.

Richins, W. D., J. C. Pechmann, R. B. Smith, C. J. Langer, S. K. Goter, J. E. Zollweg, and J. J. King (1987). The 1983 Borah Peak, Idaho, earthquake and its aftershocks, *Bull. Seismol. Soc. Am.* **77,** 694–723.

Ristau, J. (2008). Implementation of routine regional moment tensor analysis in New Zealand, *Seismol. Res. Lett.* **79,** 400–415.

Ritsema, J., and T. Lay (1995). Long-period regional wave moment tensor inversion for earthquakes in the western United States, *J. Geophys. Res.* **100,** 9853–9864.

Roller, J. C. (1965). Crustal structure in the eastern Colorado Plateau province from seismic-refraction measurements, *Bull. Seismol. Soc. Am.* **55,** 107–119.

Rowley, P. D., C. G. Cunningham, T. A. Steven, H. H. Mehnert, and C. W. Naeser (1997). Cenozoic igneous and tectonic setting of the Marysvale volcanic field and its relation to other igneous centers in Utah and Nevada, in *Laccolith Complexes of Southeastern Utah; Time of Emplacement and Tectonic Setting; Workshop Proceedings: U.S. Geological Survey Bulletin 2158*, J. D. Friedman and A. C. Huffmann (Editors), Washington 167–201.

Saikia, C. K. (1994). Modified frequency–wavenumber algorithm for regional seismograms using Filon's quadrature: Modeling of *Lg* waves in eastern North America, *Geophys. J. Int.* **118,** 142–158.

Shin, J. S., D. Sheen, and G. Kim (2010). Regional observations of the second North Korean nuclear test on 2009 May 25, *Geophys. J. Int.* **180,** 243–250.

Smith, R. B., and W. J. Arabasz (1991). Seismicity of the intermountain seismic belt, in *Neotectonics of North America: Decade Map*,

D. B. Slemmons, E. R. Engdahl, M. D. Zoback, and D. D. Blackwell (Editors), Vol. **1**, Geological Society of America, Boulder, CO, 185–228.

Song, X. J., D. V. Helmberger, and L. Zhao (1996). Broad-band modeling of regional seismograms: The basin and range crustal structure, *Geophys. J. Int.* **125,** 15–29.

Templeton, D. C., and D. S. Dreger (2006). Non-double-couple earthquakes in the Long Valley volcanic region, *Bull. Seismol. Soc. Am.* **96,** 69–79.

Thio, H. K., and H. Kanamori (1995). Moment-tensor inversions for local earthquakes using surface waves recorded at TERRAscope, *Bull. Seismol. Soc. Am.* **85,** 1021–1038.

Uhrhammer, R. A., S. J. Loper, and B. Romanowicz (1996). Determination of local magnitude using BDSN broadband records, *Bull. Seismol. Soc. Am.* **86,** 1314–1330.

Walter, F., J. F. Clinton, N. Deichmann, D. S. Dreger, S. E. Minson, and M. Funk (2009). Moment tensor inversions of icequakes on Gornergletscher, Switzerland, *Bull. Seismol. Soc. Am.* **99,** 852–870.

Walter, F., D. S. Dreger, J. F. Clinton, D. Deichmann, and M. Funk (2010). Evidence for near-horizontal tensile faulting at the base of Gornergletscher, a Swiss Alpine glacier, *Bull. Seismol. Soc. Am.* **100,** 458–472.

Zhu, L., and D. V. Helmberger (1996). Advancement in source estimation techniques using broadband regional seismograms, *Bull. Seismol. Soc. Am.* **86,** 1634–1641.

Zoback, M. L., and M. D. Zoback (1989). Tectonic stress field of the continental United States, in *Geophysical Framework of the Continental United States: Geological Society of America Memoir 172*, L. C. Pakiser and W. D. Mooney (Editors) , Geological Society of America, Boulder, CO, 523–539.

Katherine M. Whidden
Kristine L. Pankow
University of Utah Seismograph Stations
115 South 1460 East
Room 106 FASB
Salt Lake City, Utah 84112-0102 U.S.A.
whidden@seis.utah.edu